

## Black powder formation by dewing and hygroscopic corrosion processes

Martin Colahan<sup>a,b</sup>, David Young<sup>a,\*</sup>, Marc Singer<sup>a</sup>, Ricardo P. Nogueira<sup>b</sup>

<sup>a</sup> Institute for Corrosion and Multiphase Technology, Dept. of Chemical & Biomolecular Engineering, Ohio University, 342 W. State St., Athens, OH 45701, United States

<sup>b</sup> Gas Research Center, Dept. of Chemical Engineering, Khalifa University, P.O. Box 127788, Abu Dhabi, United Arab Emirates



### ARTICLE INFO

#### Keywords:

Black powder  
Internal corrosion  
Sales gas  
Dewing  
Hygroscopic  
Deliquescence

### ABSTRACT

The presence of black powder in natural gas pipelines can lead to equipment erosion, valve failure, instrumentation malfunction, and increased pressure drop. However, despite its impact on downstream and midstream operations, black powder production is poorly understood. In the present work, black powder formation as a result of corrosion was investigated by simulating sales gas conditions in a glass cell. Steel specimens were systematically exposed to a range of CO<sub>2</sub>, H<sub>2</sub>S, and O<sub>2</sub> partial pressures at differing water condensation rates. The potential for hygroscopic material assisting black powder formation was also investigated. Friable corrosion products found in dewing conditions consisted of siderite (FeCO<sub>3</sub>), mackinawite (FeS), and hematite (Fe<sub>2</sub>O<sub>3</sub>). The expected mass of corrosion products, as determined from experimental corrosion rates, are in line with the high levels of black powder that can be experienced. The presence of hygroscopic NaCl crystals facilitated corrosion at relative humidities as low as 33%.

### 1. Introduction

Black powder, particles which can be entrained by a natural gas stream, is a common problem in natural gas pipelines and if left unchecked can erode equipment, induce greater pressure drops, and clog instrumentation (Baldwin, 1997). Black powder may contain corrosion products, salt, dirt, and other materials such as those trapped in the pipeline during construction. Previous studies examining the composition of black powder have found primarily iron oxides and iron sulfides, but iron oxyhydroxides, iron carbonate, and elemental sulfur were also reported (Bhardwaj et al., 2016; Khan et al., 2015; Sherik et al., 2008; Yamada et al., 2011). The frequent occurrence of the aforementioned species have led researchers to conclude black powder is predominantly a result of corrosion (Baldwin, 1997; Bhardwaj et al., 2016; Khan and Al-Shehhi, 2015; Khan et al., 2015; Sherik et al., 2008; Yamada et al., 2011).

Corrosion in natural gas pipelines is typically caused by the presence of CO<sub>2</sub>, H<sub>2</sub>S, and O<sub>2</sub> with liquid water. CO<sub>2</sub> and H<sub>2</sub>S are known to be present within natural gas at various concentrations, but O<sub>2</sub> is rarely reported. Exogenous oxygen ingress is attributed to be the primary source of O<sub>2</sub> in natural gas and can lead to concentrations ranging from 0 to 0.03 vol% (Sherik et al., 2008; Sridhar et al., 2001). Liquid water may seldom occur as the gas is dehydrated to 7 lbs H<sub>2</sub>O/MMscf (0.112 mg/l) or lower to reduce the risk of internal corrosion, however, upsets in gas dehydration units may release enough water for condensation to be feasible. Measured dew points of water in the sales gas

network were reported by Sherik et al. (Sherik et al., 2008) The sales gas moisture content consistently exceeded the maximum moisture level of 7 lbs/MMscf (0.112 mg/l) risking dew formation. The measured water dew points were compared to meteorological data to examine the potential for water condensation on the steel pipeline. Winter ambient temperatures were frequently below the water dew point temperatures measured, therefore, water condensation was deemed likely.

Water accumulation at the steel wall may be facilitated if a hygroscopic material such as salt is present on the steel surface. The frequent use in some regions, in particular arid locations, of seawater as an economical hydrotest medium can leave a hygroscopic salt residue on the steel surface once the water is removed unless rinsed properly (Hali et al., 2016; Holden et al., 2010; Zhao et al., 2010). The presence of salts in regions associated with black powder formation has also been attributed to production water carryover in a case study on the mitigation of black powder production in the field (Olabisi et al., 2017). This salt layer can attract and accumulate water potentially deliquescing in the process. In oxic environments, the presence of hygroscopic NaCl particles on mild steel led to corrosion in relative humidities as low as 33%, much lower than the NaCl deliquescence relative humidity of 75% (Schindelholz et al., 2014). Hygroscopic corrosion in CO<sub>2</sub>/H<sub>2</sub>S conditions is even less well studied. Corrosion in non-saturated conditions was observed in CO<sub>2</sub> and CO<sub>2</sub>/H<sub>2</sub>S (Kolts, 2004; Litke et al., 2013), but neither morphology nor corrosion product composition were analyzed so the potential for black powder production through hygroscopic corrosion processes remains unknown.

\* Corresponding author.

E-mail address: [youngd1@ohio.edu](mailto:youngd1@ohio.edu) (D. Young).

**Table 1**  
Sponsor-provided sales gas conditions.

Parameter	Value
CO <sub>2</sub> Content	1.31 mol%
H <sub>2</sub> S Content	7 ppm
Operating Temperature	33–50 °C
Operating Pressure	40–42 bar
Flow Rate	550 MMscfd (180 sm <sup>3</sup> /s)
Pipeline Diameter	42 (106.7) Inches (cm)

Water availability has been identified as the primary unknown for corrosion in sales gas conditions since the concentrations of CO<sub>2</sub>, H<sub>2</sub>S, and O<sub>2</sub> are known to be adequate for corrosion to occur. If the water content of the sales gas is high, then water may condense onto the steel surface. However, if the water content is below the thermodynamic dew point temperature, then a hygroscopic material like salt must be present for corrosion to occur. Largely absent from the black powder literature is information relating to corrosion product spallation. A corrosion product layer can grow in a pipeline, but if that corrosion product cannot spall then it cannot become entrained in the gas thus forming black powder. In CO<sub>2</sub>/H<sub>2</sub>S conditions related to sales gas pipelines experiencing dewing corrosion, friable FeS layers were observed (Yaakob et al., 2016). Similar layers may be formed in sales gas conditions which may ultimately lead to black powder formation. H<sub>2</sub>S partial pressure and water condensation rate were critical to the development of the friable layers but were little explored. The effect of CO<sub>2</sub>, H<sub>2</sub>S, and O<sub>2</sub> concentrations on the development of corrosion product layers due to dewing and hygroscopic corrosion are explored in the present study.

## 2. Experimental procedure

Corrosion in sales gas conditions was examined by exposing X65 steel specimens to CO<sub>2</sub>/H<sub>2</sub>S or CO<sub>2</sub>/O<sub>2</sub> mixtures in dewing or hygroscopic conditions. Gas concentrations were derived from sales gas conditions supplied by the sponsor as shown in Table 1; O<sub>2</sub> and H<sub>2</sub>O concentrations were not supplied.

From the specified gas concentrations and the highest operating pressure, the partial pressures of CO<sub>2</sub> and H<sub>2</sub>S were calculated to be approximately 0.55 bar and 0.3 mbar, respectively. To investigate the effect of H<sub>2</sub>S content, the H<sub>2</sub>S partial pressures tested were 0, 0.1, 0.3, and 1.0 mbar. The H<sub>2</sub>S was diluted with CO<sub>2</sub> for CO<sub>2</sub> partial pressures of 0.96–0.98 bar. Corrosion at 0.1–1 mbar H<sub>2</sub>S is known to be H<sub>2</sub>S dominant, so dilution over the 0.55 bar CO<sub>2</sub> partial pressure should not affect results. Tests with O<sub>2</sub> were conducted at 10 mbar O<sub>2</sub>, the partial pressure expected if the O<sub>2</sub> content was ca. 0.02 mol%. Gas flow rates were kept low so that the specimens experience a largely quiescent gas environment.

Experiments were conducted with API<sup>1</sup> 5L X65 steel specimens. The specimens were machined into two geometries: 1.25-inch-diameter × 0.5-inch-thick (31.7 mm × 12.7 mm) cylindrical specimens for surface and corrosion rate analysis, and 0.5 × 0.5 × 0.08 inch<sup>3</sup> (12.7 × 12.7 × 2 mm<sup>3</sup>) specimens for XRD analyses. Specimens were coated with a fluoropolymer to prevent corrosion on undesired surfaces and eliminate galvanic effects. The composition of the steel is shown in Table 2. As the H<sub>2</sub>S partial pressures used during experimentation fall below the 0.3 kPa guideline for CRAs as noted in NACE MR0175/ISO15156, low-carbon steel usage can be expected under these conditions (NACE MR0175, 2015).

### 2.1. Dewing corrosion apparatus and experimental procedure

Dewing conditions were examined by exposing steel specimens to water-saturated CO<sub>2</sub>, CO<sub>2</sub>/H<sub>2</sub>S or CO<sub>2</sub>/O<sub>2</sub> mixtures in the apparatus shown in Fig. 1. The apparatus and procedures for testing in dewing conditions are based largely on those used by Yaakob et al. (Yaakob et al., 2016), to test marginally sour TLC conditions, though modifications were made to better control the steel temperature and therefore the water condensation rate. Experiment selection was guided by the test matrix shown in Table 3.

Gas, metered by a rotameter, at the desired CO<sub>2</sub>, H<sub>2</sub>S, and O<sub>2</sub> concentrations, was bubbled through 1 L of heated deionized (DI) water located in the bottom of the glass cell to heat and saturate the gas with water. The temperature of the water, which is controlled by the hot-plate, is set such that the gas above the solution near the specimens is held at the desired temperature of 30 °C. Gas was bubbled through the glass cell for a minimum of 3 h before the steel specimens were inserted.

One large cylindrical specimen and one XRD specimen were included in each test. The specimens were then ground with silicon carbide abrasive papers to a 600 grit finish with water as the coolant. The water was rinsed from the surface with isopropanol immediately after grinding to minimize unwanted corrosion. The specimens were cleaned in isopropanol in an ultrasonic bath, dried with cool air, and then the initial mass was recorded. Specimens were stored in nitrogen until insertion, which was ordinarily less than an hour after polishing. The cylindrical specimens were inserted directly into PEEK specimen holders designed to provide a gas-tight seal to the lid. The smaller XRD specimens were suspended from the lid with a specially designed holder where the steel specimen was held by a magnet within an aluminum body which aids heat transfer to the temperature control system. Peltiers and heatsinks were placed over the specimens, and the resultant stack was fastened to the lid. Temperature control was then initiated to cool the specimens to 25 or 15 °C to achieve the low water condensation rate (WCR) of 0.015 ml/m<sup>2</sup>/s or high WCR of 0.05 ml/m<sup>2</sup>/s, respectively. The WCRs were calculated with an in-house water condensation model.

Specimen temperature control was performed with a PID controller. Steel temperature was measured with 10 kΩ thermistors mounted to the side of the cylindrical specimens or within the aluminum body of the XRD specimen holder. Peltiers held in thermal contact with the specimen facilitates cooling by acting as a heat pump when electrical power is applied. By controlling the amount of power supplied to the Peltier, the amount of heat transferred can be controlled. Power to the Peltiers is supplied by an external AC to 12 V DC power supply controlled with pulse width modulation to the duty cycle determined with the PID algorithm. During operation, a significant amount of heat is generated, so a water-cooled heatsink is placed over the Peltier to prevent overheating. Additionally, a double-pole-double-throw mechanical relay was installed between the controller and the Peltier to more easily switch the polarity of the Peltier, if necessary.

After specimen insertion, the glass cell was allowed to purge for an additional 30 min with CO<sub>2</sub> before H<sub>2</sub>S was then added into the system, when required. The H<sub>2</sub>S concentration was set by mixing a CO<sub>2</sub> and a premixed CO<sub>2</sub>/H<sub>2</sub>S stream metered by a rotameter upstream of the glass cell. The H<sub>2</sub>S concentration was measured with colorimetric gas detector tubes and adjusted as necessary. The desired oxygen concentration was achieved by mixing CO<sub>2</sub> and air in the same manner as CO<sub>2</sub>/H<sub>2</sub>S. The O<sub>2</sub> partial pressure was measured with an O<sub>2</sub> analyzer throughout the experiment and adjusted as needed. Gas was continuously passed through the glass cell throughout the experiments. Effluent gas containing H<sub>2</sub>S was vented through a sodium hydroxide solution then an activated carbon scrubber. Test conditions were monitored and adjusted as needed to maintain experimental parameters.

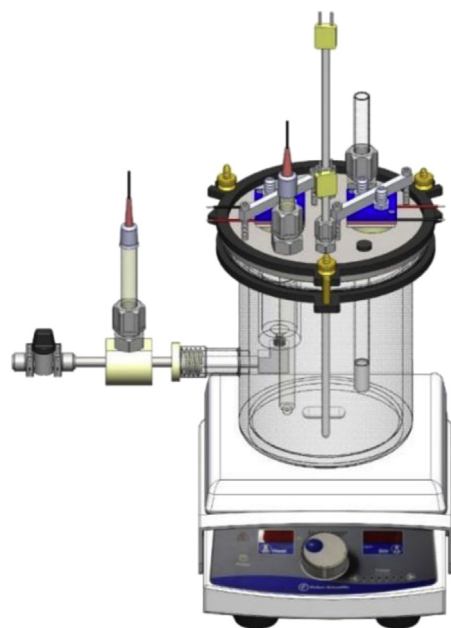
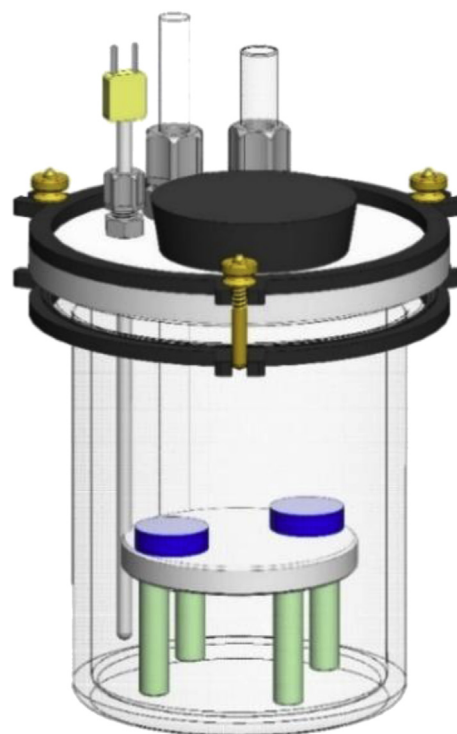
After the allotted exposure time, the specimens were removed and immediately rinsed with isopropanol to remove water and prevent

<sup>1</sup> American Petroleum Institute (API), 1220 L St. NW, Washington, DC 20005.

**Table 2**

Composition of API 5L X65 steel (wt%, balance Fe).

C	Mn	Mo	Ni	Cu	S	V	Si	Co	Al	P	Sb	As	Sn	Zn	Nb	Ti
0.05	1.21	0.16	0.38	0.14	< 0.001	0.04	0.25	0.012	0.033	0.004	0.035	0.015	0.012	0.004	0.03	0.01

**Fig. 1.** Dewing corrosion apparatus.**Fig. 2.** Hygroscopic corrosion glass cell.**Table 3**

Dewing corrosion test matrix.

Parameter	Value
Test Material	API 5L X65
Total Pressure (bar)	1
H <sub>2</sub> S Partial Pressure (mbar)	0, 0.1, 0.3, 1.0
O <sub>2</sub> Partial Pressure (mbar)	0, 10
CO <sub>2</sub> Partial Pressure (bar)	0.96, 0.92
N <sub>2</sub> + Ar Partial Pressure (bar)	0, 0.04
Test Duration (days)	0.25, 1, 3, 7, 10
Water Condensation Rate (ml/m <sup>2</sup> /s)	0.015, 0.05
Steel Temperature (°C)	25, 15
Gas Temperature (°C)	30

unwanted oxidation. The rinse was performed by targeting the top of the specimen with a stream of isopropanol from a squirt bottle, allowing the isopropanol to drench the rest of the specimen. The specimens were dried under nitrogen, optical images taken, and specimens with corrosion product weighed. The specimens were then stored in a desiccator under nitrogen awaiting further analysis.

## 2.2. Hygroscopic corrosion apparatus and experimental procedure

Hygroscopic corrosion tests were performed in a glass cell with the specimens located on a platform above the saturated salt solutions at the bottom, as shown in Fig. 2. The apparatus consisted of a glass cell, lid, lid clamp, gas inlet, gas outlet, specimen platform, thermocouple, and a saturated salt solution to control the relative humidity (RH). A large hole was made in the lid for fast specimen insertion and extraction. The large hole was sealed with a rubber stopper which was clamped down, if necessary, to ensure a gas-tight seal. Prior to testing, the glass cell, lid and stage were thoroughly cleaned with deionized (DI) water and isopropanol then dried. In the bottom of the glass cell, 100 ml of DI water was mixed with salt at 125% of the solubility limit in water

**Table 4**

Hygroscopic corrosion test matrix.

Parameter	Value
Test Material	API 5L X65
Total Pressure (bar)	1
H <sub>2</sub> S Partial Pressure (mbar)	0.3
O <sub>2</sub> Partial Pressure (mbar)	0
CO <sub>2</sub> Partial Pressure (bar)	0.97
N <sub>2</sub> + Ar Partial Pressure (bar)	0
Test Duration (days)	3
Relative Humidity (%)	75, 58, 33
Saturated Salt	NaCl, NaBr, MgCl <sub>2</sub>
Salt Layer	NaCl
Temperature (°C)	25

at 25 °C. The stage was then placed into the glass cell and the lid was fastened. The glass cell is purged with N<sub>2</sub> for a minimum of 5 h to remove oxygen. The test matrix for the hygroscopic corrosion experiments is shown in Table 4.

A cylindrical specimen and an XRD specimen were included in each test. The steel surface was ground with carbide abrasive paper and then polished to a mirror finish with a 0.25 μm diamond suspension. The specimens were then thoroughly rinsed with DI water and isopropanol then ultrasonically cleaned in isopropanol. The specimens were dried with cool air, and the specimen mass was recorded. The specimens were stored in N<sub>2</sub> until salt was deposited onto the surface.

Salt layers were generated by drying an aqueous NaCl solution placed on preweighed steel specimens under N<sub>2</sub>. A 3.5 wt% NaCl solution was prepared prior to experimentation and used for all experiments; this is a similar salinity to seawater. The salt solution was purged

with  $N_2$ , and 250  $\mu$ l of solution was deposited onto the steel surface with a pipette. The specimen was immediately placed in a  $N_2$  environment, and the water was then spread over the entire surface by tilting the specimens. The salt solution was dried by passing dry  $N_2$  over the wetted steel surface. Once the salt crystallized, the specimen with salt was weighed, photographed, and then placed in the  $N_2$ -purged glass cell on the platform salt-side up. Approximately 0.010 g NaCl was placed on each cylindrical specimen. The possibility of corrosion during the salt-drying process was examined by SEM surface analysis after removing the dried NaCl layer with DI water followed by an isopropanol rinse and drying with  $N_2$ .

The glass cell was allowed to purge with  $N_2$  for another 30 min before replacement with the test gas which was continuously sparged into the system throughout each experiment. The dry test gas entered the glass cell through a tube with the outlet approximately 1 cm above the saturated salt solution. The gas was not bubbled through the salt solution to prevent aerosol formation which can contaminate the steel surface; this phenomenon was observed in preliminary experiments with saturated  $MgCl_2$ . A small gas flow rate was maintained throughout the experiment to prevent a decrease in the gas RH. In sweet conditions, a hygrometer was placed downstream of the glass cell to verify the relative humidity (the hygrometer could not be used in  $H_2S$  testing due to chemical incompatibilities). Specimen extraction was performed in the same manner as outlined in the dewing corrosion procedures.

### 2.3. Analytical methods

Scanning electron microscopy (SEM) was performed to examine the corrosion product morphology. Hygroscopic corrosion specimens were sputter coated with palladium to minimize charging in the SEM. Corrosion product/phase composition was determined with Raman spectroscopy and X-ray diffraction (XRD). Raman spectroscopy was conducted with a 785 nm wavelength laser. XRD was performed with a  $CuK_{\alpha}$  source over  $10$ – $70^\circ$   $2\theta$  at a scan rate of  $1^\circ$  per minute. The corrosion product was removed in accordance with ASTM<sup>2</sup> G1-03 (Standard Practice for Preparing, Cleaning and Evaluating Corrosion Test Specimens, 2011), and the corrosion rate and corrosion product mass was calculated by comparing the after removal mass to the initial mass and the after extraction mass, respectively.

## 3. Results and discussion

### 3.1. Dewing corrosion

The effect of  $H_2S$  partial pressure ( $p_{H_2S}$ ) was examined by exposing the steel specimens to differing  $H_2S$  concentrations in the absence of  $O_2$  at the low WCR for 3 days. The effect of  $H_2S$  partial pressure on the corrosion product morphology is shown in Fig. 3.

Little corrosion product was observed in the absence of  $H_2S$ , but a spalling corrosion product was obtained in the experiments with  $H_2S$ . At 0.1 mbar  $H_2S$ , buckles in the FeS layer leading to cracking were observed, but those regions were generally relegated to regions which are presumed to be the edges of water droplets. At higher  $H_2S$  partial pressures, FeS spallation was much more pronounced. Greater buckling was found at 0.3 mbar  $H_2S$  than at 0.1 mbar, though they were again generally confined to specific regions. At 1.0 mbar  $H_2S$  severe buckling was observed over the specimen surface.

Diffraction patterns of specimens recovered from the  $H_2S$  experiments examining the effect of  $p_{H_2S}$  are shown in Fig. 4. XRD did not pick up any corrosion product on the specimen analyzed from the  $CO_2$  experiment, but mackinawite (FeS) was detected in tests with  $H_2S$ . Increasing the  $H_2S$  partial pressure saw an increase in mackinawite peak intensity, but the relative peak intensities did not match the reference

(Lennie et al., 1995) indicating preferred orientation in the mackinawite layer. This has been postulated to be due to a growth mechanism favoring parallel [100] and [001] iron and mackinawite planes, respectively.

The effect of  $H_2S$  concentration on corrosion rate is shown in Fig. 5(a). The addition of 0.1 and 0.3 mbar  $H_2S$  generally decreased the corrosion rate due to the corrosion product offering more protection. However, increasing the  $H_2S$  partial pressure to 1.0 mbar  $H_2S$  saw a large increase in the corrosion rate. This is presumed to be due to the much higher degree of spallation observed at 1.0 mbar  $H_2S$  than at 0.3 and 0.1 mbar  $H_2S$  since a spalling layer cannot offer as much protection to the steel as a more stable layer.

The measured corrosion product mass, theoretical corrosion product mass, and maximum black powder production rate after 3 days are shown in Fig. 5(b). The measured corrosion product mass is determined by the mass of corrosion product removed, and the theoretical corrosion product is determined by calculating the mass of corrosion product possible from the iron lost due to corrosion by the methodology described in Appendix A. Since the experiments were performed in the absence of oxygen, corrosion product identity was assumed to be  $FeCO_3$  in  $H_2S$ -free conditions and FeS in  $H_2S$ -containing conditions. Most of the iron available for corrosion product formation on the steel surface was not present in the measured corrosion product as it either dripped away with condensed water as aqueous  $Fe^{2+}$  or was present in spalled corrosion product. The difference in the theoretical and measured corrosion product masses generally decreased with increasing  $H_2S$  concentration, but this is expected since corrosion product layers are easier to produce in sour systems than sweet systems at the temperatures tested. The maximum black powder production rate, plotted on the secondary axis in red, is calculated by extrapolating the theoretical corrosion product mass averaged by the experimental duration to a 100 km segment of a 42 inch (106.7 cm) ID pipeline. The maximum black powder production rates varied from 900 to 2000 kg/day for a 100 km, 42 inch ID pipeline. These numbers are high, but they represent a worst-case scenario where the entire pipeline is experiencing water condensation.

The effect of time was examined by exposing steel specimens to 0.3 mbar  $H_2S$  and 0.96 bar  $CO_2$  in an  $O_2$ -free environment for up to 10 days. Time dependency relating to corrosion rate, measured and theoretical corrosion product mass, and maximum black powder production rate is shown in Fig. 6. The corrosion rate decreased with time from 0.28 mm/yr to a steady corrosion rate of 0.10 mm/yr after the corrosion product had time to develop. The measured corrosion product mass gradually increased with time as the corrosion rate reached a steady value, the estimated maximum black powder production rate flattened at ca. 1000 kg/day for a 100 km, 42 in. ID pipeline.

The effect of time on the corrosion product layer morphology is shown in Fig. 7. After 6 h, the only visible corrosion product was confined to the structures shown. Flakes were already beginning to form, but no buckling was observed. FeS layer buckling was evident after 1 day where the buckled corrosion product was evident only surrounding the flakey structures seen after 6 h. The severity of buckling intensified with time developing large buckled regions after 7 days. Similar sized features were not observed after 10 days as they likely had been removed from the surface.

The effect of WCR was investigated by exposing steel specimens to the high and low WCR of 0.05 and 0.015 ml/m<sup>2</sup>/s, respectively, at 0 and 0.3 mbar  $H_2S$ . The corrosion product morphology is shown in Fig. 8. In sweet conditions, the corrosion product morphology was consistent with iron carbide, which is exposed in a ferritic material as iron is removed due to corrosion. The lack of iron carbonate suggests either solubility requirements and/or precipitation kinetics were not sufficient for meaningful precipitation. At 0.3 mbar  $H_2S$  – 0.05 ml/m<sup>2</sup>/s WCR, buckled corrosion products were present.

The effect of WCR on corrosion rate, corrosion product mass, and maximum allowable black powder production rate is shown in Fig. 9.

<sup>2</sup> ASTM International, 100 Barr Harbor Dr., West Conshohocken, PA 19428–2959.

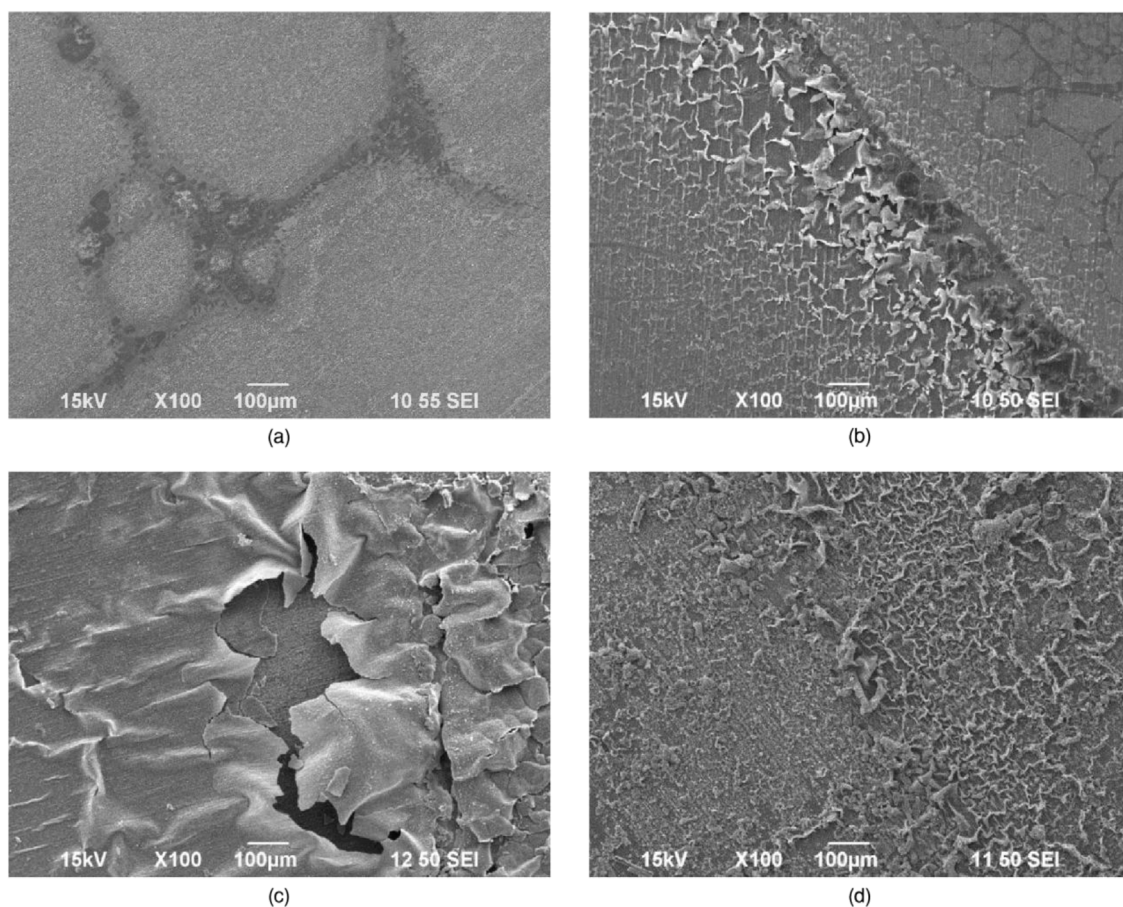


Fig. 3. Effect of  $H_2S$  partial pressure on the morphology of corrosion products produced after 3 days under dewing conditions with (a) 0 mbar  $H_2S$ , (b) 0.1 mbar  $H_2S$ , (c) 0.3 mbar  $H_2S$ , and (d) 1.0 mbar  $H_2S$ . (Common conditions: X65 steel, 3 days, 0.96 bar  $CO_2$ , 0.015 ml/m<sup>2</sup>/s WCR, 30 °C  $T_{gas}$ , 25 °C  $T_{steel}$ ).

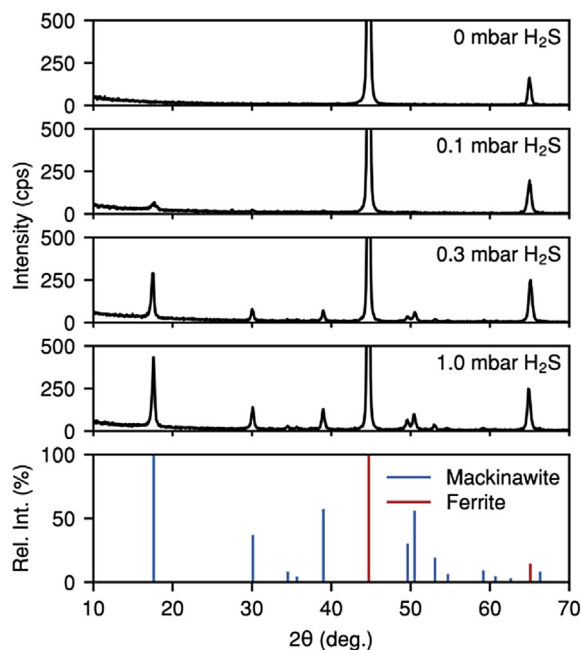


Fig. 4. XRD analysis on the effect of  $H_2S$  partial pressure on the composition of corrosion products produced after 3 days under dewing conditions. (Common conditions: X65 steel, 3 days, 0.96 bar  $CO_2$ , 0.015 ml/m<sup>2</sup>/s WCR, 30 °C  $T_{gas}$ , 25 °C  $T_{steel}$ ).

While little difference in corrosion rate is observed at 0.3 mbar  $H_2S$ , the corrosion rate increased by 70% in the absence of  $H_2S$ . The difference in corrosion rates in sweet conditions is largely due to water chemistry. The higher WCR allows for lower  $Fe^{2+}$  concentrations and a lower bulk pH creating a more corrosive environment. The sour systems were not as affected by the increase in WCR as FeS layers were present regardless of WCR.

The increased degree of buckling over time in the FeS layers is related to the accumulation of compressive stress following the FeS layer growth. Consequently, buckling appears as a spontaneous mechanism of releasing the energy stored in the corrosion product layer. Stress accumulation may be caused through a variety of pathways. In the Sun-Nesic model (Sun and Nešić, 2009) of iron sulfide layer formation, stress accumulation which leads to cracking and spallation is due to volume differences between the ferrite and the mackinawite (Sun and Nešić, 2009). The ratio of the scale volume to the substrate volume, more commonly known as the Pilling-Bedworth ratio (PBR) (Bedworth and Pilling, 1923), for FeS relative to ferrite is about 2.6. Since the PBR is greater than 1, compressive stress within the layer is expected to accumulate and lead to layer failure. However, the PBR is not especially useful for layers grown through outward cation diffusion, which is the case for most sulfides. Layers grown via outward cation diffusion can grow outward from the scale surface and, therefore, are not volume limited as required to apply the PBR (Birks et al., 2006).

Sun and Nesic suggest epitaxial stresses which arise due to unit cell size differences may lead to stress accumulation (Sun and Nešić, 2009). However, the adherence of the sulfide to the metal is expected to be fairly weak due to void formation as the steel substrate corrodes which may limit epitaxial stresses (Birks et al., 2006). A perhaps more plausible method of stress accumulation may be due to crystal growth at

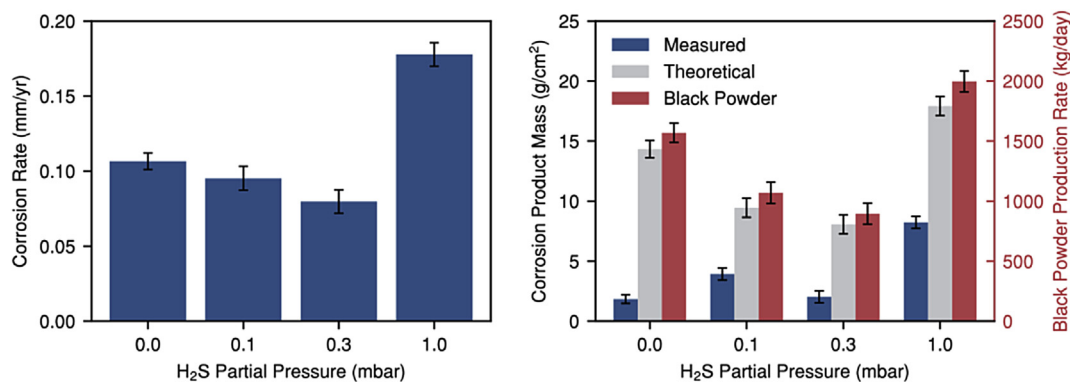


Fig. 5. Effect of H<sub>2</sub>S partial pressure on (a) corrosion rate and (b) measured and theoretical corrosion product mass (left axis) and maximum allowable black powder production rate (right axis). The calculation for black powder production rate assumes a straight, 42 in. (1.07 m) ID, 100 km pipeline. (Common conditions: X65 steel, 0.96 bar CO<sub>2</sub>, 0.015 ml/m<sup>2</sup>/s WCR, 30 °C T<sub>gas</sub>, 25 °C T<sub>steel</sub>, 3 days).

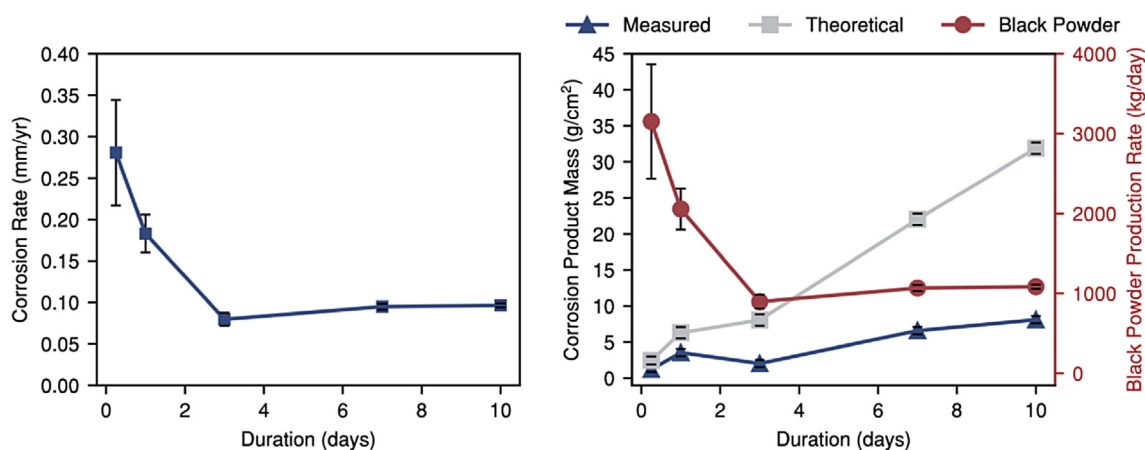


Fig. 6. Effect of time on corrosion rate, corrosion product mass (left axis), and maximum allowable black powder production rate (right axis) at 0.3 mbar pH<sub>2</sub>S under dewing conditions. The calculation for black powder production rate assumes a 42 in. (1.07 m) ID, 100 km pipeline. (Common conditions: X65 steel, 0.3 mbar H<sub>2</sub>S, 0.96 bar CO<sub>2</sub>, 0.015 ml/m<sup>2</sup>/s WCR, 30 °C T<sub>gas</sub>, 25 °C T<sub>steel</sub>).

cracks or grain boundaries. Crystal growth due to the addition of ferrous and sulfide ions to an already formed crystal may lead to crystals pushing against one another therefore compressively stressing the layer. Crystal growth at grain boundaries and cracks has been used to explain the buckling of chromium oxide scales and oxide scales on Fe-Cr-Al alloys (Birks et al., 2006; Golightly et al., 1979; Kofstad and Lillerud, 1980; Lillerud and Kofstad, 1980).

In all H<sub>2</sub>S experiments, black particles were present in collected fluid after the isopropanol rinse of extracted specimens. The wall shear stress imposed by the isopropanol was estimated to be approximately 1 Pa based on the flow of a falling laminar film (Bird et al., 2007). This shear stress is similar to the wall shear stress expected based on the conditions in Table 1. It is unlikely this small shear stress would cause damage to a corrosion product layer experiencing little to no intrinsic stress, so it is postulated that black powder formation due to H<sub>2</sub>S is predominantly caused by intrinsic stresses within the layer generated by layer growth rather than the extrinsic stresses caused by fluid flow. This is a point of major concern as it indicates that black powder release inside operating pipelines cannot be avoided by solely tuning operational parameters, such as fluid velocity or flow regime, but must instead be mitigated in the first stages of layer formation. Black powder mitigation through the use of appropriate corrosion inhibitors is a subject of ongoing work in our research groups. It is important to note that all corrosion product layers were generated under largely quiescent conditions. The addition of flow during the formation of corrosion products is hypothesized to yield a higher corrosion rate as the steel is left more unprotected as the corrosion product is sheared off the steel

surface thereby increasing the potential for black powder formation. This is a topic of ongoing research.

The effect of oxygen was examined by exposing steel specimens at the low WCR of 0.015 ml/m<sup>2</sup>/s to a CO<sub>2</sub>/O<sub>2</sub> mixture with a 10 mbar O<sub>2</sub> partial pressure. The addition of oxygen to a CO<sub>2</sub> environment saw, as expected, a dramatic increase in corrosion rate and corrosion product mass as shown in Fig. 10.

The dramatic increase in the corrosion rate and corrosion product mass resulted in development of a bilayered corrosion product, as shown in Fig. 11(a). The inner layer was well adhered to the steel, but the outer layer was more loosely bound. The outer layer is presumed to have grown on the gas/liquid interface since a flat surface is present on the outer layer whereas the inner layer is more rough. Red flakes of corrosion product were observed in the collected isopropanol after rinsing which suggests black powder components would readily detach in oxic conditions.

Seemingly contradictory results were obtained from corrosion product composition analysis with XRD and Raman spectroscopy as shown in Fig. 11(b) and (c), respectively. Siderite (FeCO<sub>3</sub>) was detected with XRD, but hematite (Fe<sub>2</sub>O<sub>3</sub>) was detected by Raman spectroscopy. It is postulated that an amorphous or nanocrystalline hematite layer was present on the corrosion product surface which cannot be detected by XRD but is detected by the more surface sensitive Raman characterization technique.

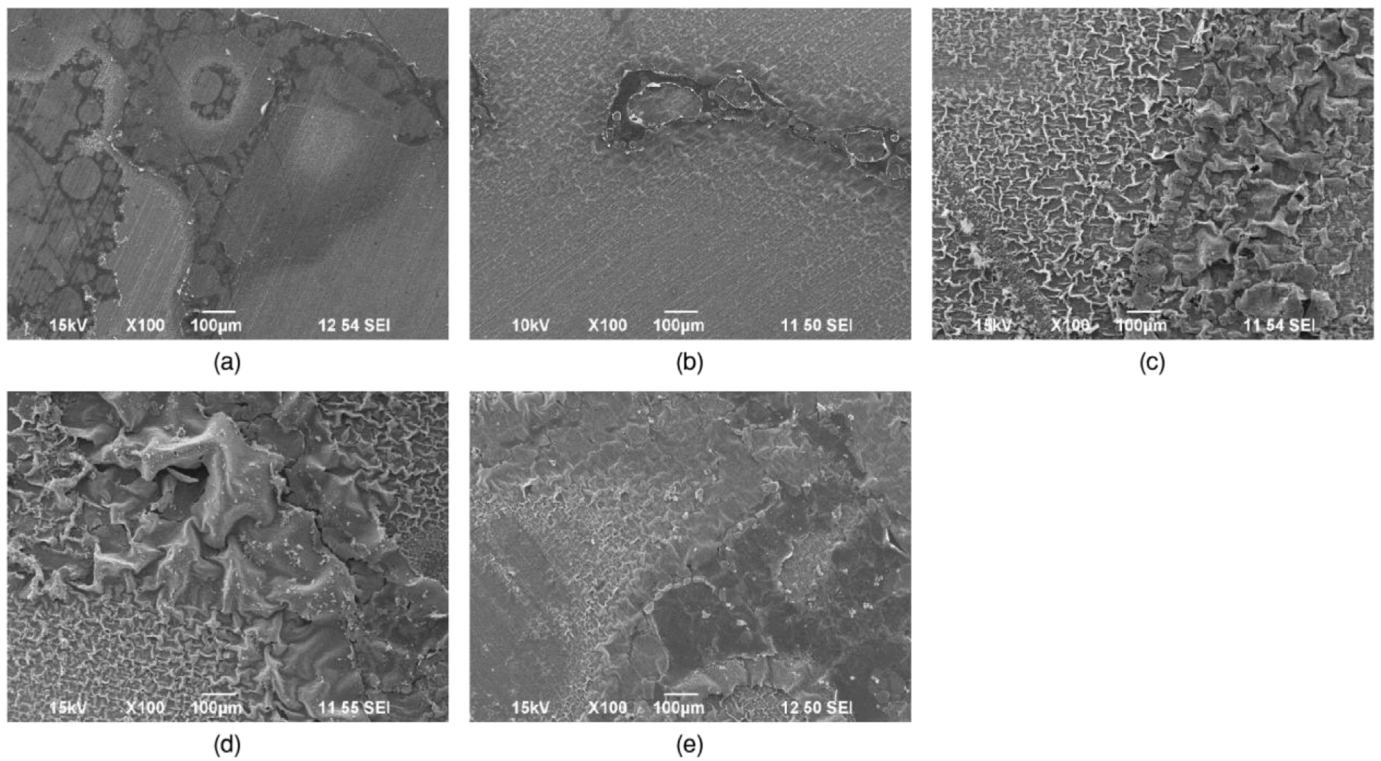


Fig. 7. Effect of time on the morphology of corrosion products produced a (a) 6-h, (b) 1-day, (c) 3-day, (d) 7-day, and (e) 10-day exposure to dewing conditions at 0.3 mbar H<sub>2</sub>S under the low water condensation rate. (Common conditions: X65 steel, 0.3 mbar H<sub>2</sub>S, 0.96 bar CO<sub>2</sub>, 0.015 ml/m<sup>2</sup>/s WCR, 30 °C T<sub>gas</sub>, 25 °C T<sub>steel</sub>).

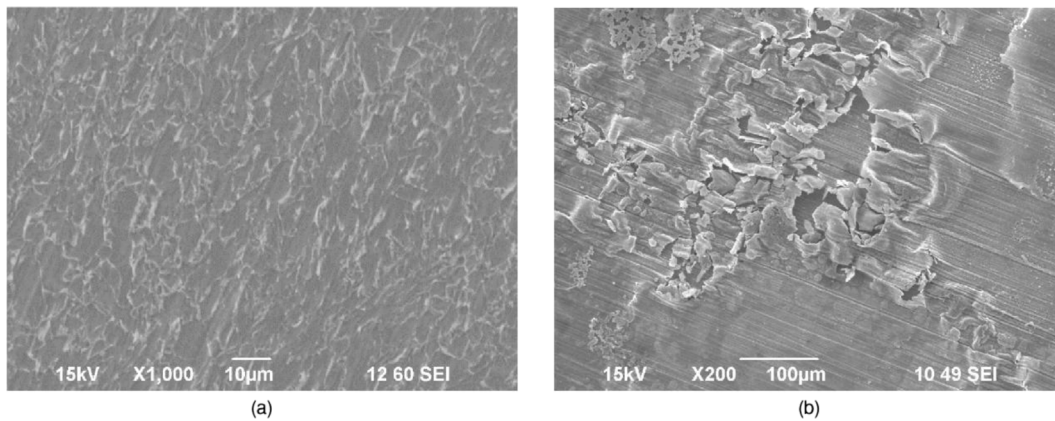


Fig. 8. Corrosion products produced under the high water condensation rate at 0 and 0.3 mbar H<sub>2</sub>S. (Common conditions: X65 steel, 0.96 bar CO<sub>2</sub>, 0.05 ml/m<sup>2</sup>/s WCR, 30 °C T<sub>gas</sub>, 15 °C T<sub>steel</sub>).

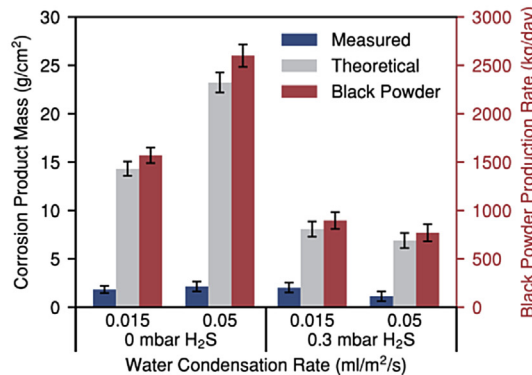
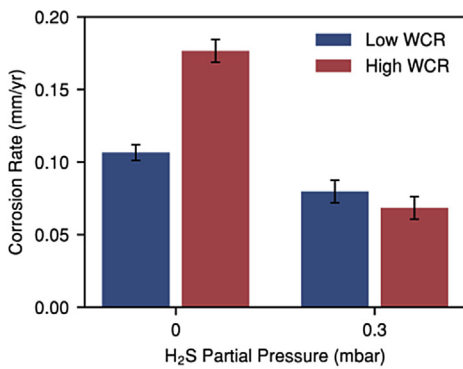
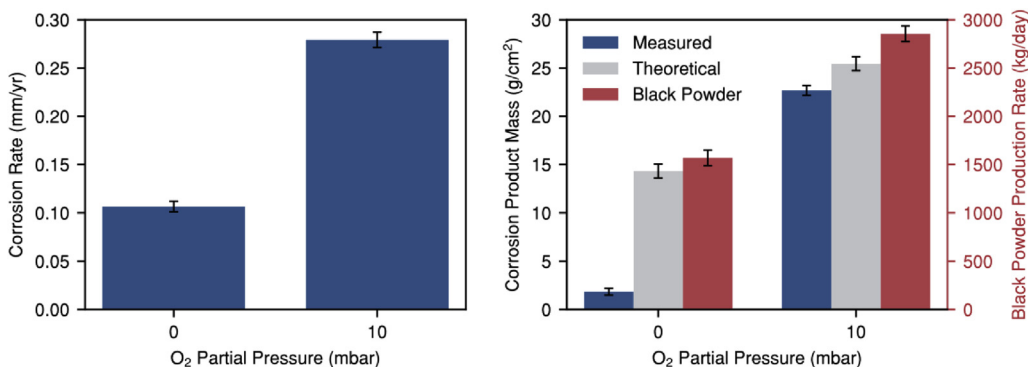


Fig. 9. Effect of water condensation rate on corrosion rate, corrosion product mass (left axis), and maximum black powder production rate (right axis) under CO<sub>2</sub> and 0.3 mbar H<sub>2</sub>S conditions. The calculation for black powder production rate assumes a 42 in. (1.07 m) ID, 100 km pipeline. (Common conditions: X65 steel, 0.96 bar CO<sub>2</sub>, 30 °C T<sub>gas</sub>).



**Fig. 10.** Effect of  $O_2$  on corrosion rate, corrosion product mass (left axis), and maximum black powder production rate (right axis) under sweet conditions. The calculation for black powder production rate assumes a 42 in. (1.07 m) ID, 100 km pipeline. (Common conditions: X65 steel, 0.96 bar  $CO_2$ , 0 mbar  $pH_2S$ , 0.015 ml/ $m^2/s$  WCR, 25 °C  $T_{steel}$ , 30 °C  $T_{gas}$ ).

### 3.2. Hygroscopic corrosion

The presence of hygroscopic material such as a salt is hypothesized to sustain corrosion in water unsaturated conditions which can lead to black powder formation. NaCl was deposited onto the surface of freshly polished steel specimens and the specimens were exposed to a 0.3 mbar  $H_2S/CO_2$  environment at 75, 58, and 33% relative humidity (RH). The effect of the exposure is investigated in Fig. 12. The salt layer exhibited a cubic morphology typical of NaCl crystals as shown in Fig. 12(a). Slight corrosion did occur during the drying process as evident by the localized features in locations presumed to be where the salt crystal perimeter once was in Fig. 12(b). No mass change was measured because of this corrosion.

After the 3-day exposure, corrosion product formation was apparent at 75% RH, Fig. 12(c), where the salt on the steel specimen deliquesced. Corrosion around a salt crystal resulting in a thin, flakey shell of corrosion product after the salt had completely deliquesced. Corrosion is not as obvious in the specimens exposed to the 58 and 33% RH based on SEM, but is still apparent.

The effect of RH on corrosion rate, corrosion product mass, and maximum allowable black powder production rate is shown in Fig. 13. The corrosion rate saw a large drop as the RH fell below the deliquescence relative humidity (DRH) of NaCl (75% RH), however, corrosion was still sustained down to 33% RH. The measured corrosion product mass was higher than the theoretical mass, but this is likely due to the presence of NaCl in the measured corrosion product which was not quantified.

The presence of a hygroscopic salt on the steel surface has led to the development of a flakey corrosion product layer at the salt DRH.

Whether or not this layer could spall to form black powder is still unknown. At relative humidities lower than the DRH, corrosion occurred, but the corrosion product is less likely to spall without external assistance such as from an impinged particle.

### 4. Conclusions

- ❖ The presence of  $H_2S$  in dewing systems developed corrosion product layers that were prone to buckling and spallation due to compressive stress generated during layer growth. The degree of FeS layer spallation increased with increasing  $H_2S$  partial pressure and increasing time suggesting spallation is coupled with growth of the layer.
- ❖ Black powder formation from FeS corrosion product layers is caused predominantly by intrinsic stresses rather than extrinsic stresses.
- ❖ The addition of  $O_2$  into sweet systems lead to a dramatic increase in corrosion rate and corrosion product mass, but the corrosion product was predominantly siderite though hematite was also detected.
- ❖ Corrosion occurred in non-water saturated conditions as low as 33% RH, however, friable corrosion products were limited to conditions experiencing a liquid layer on the surface.
- ❖ Maximum possible black powder production rates achieved a steady-state value of approximately 1000 kg/day for the hypothetical pipeline considered (100 km, 42 in. ID).
- ❖ A potential strategy to prevent black powder formation is the use of inhibitors which target the first stages of corrosion product layer formation.

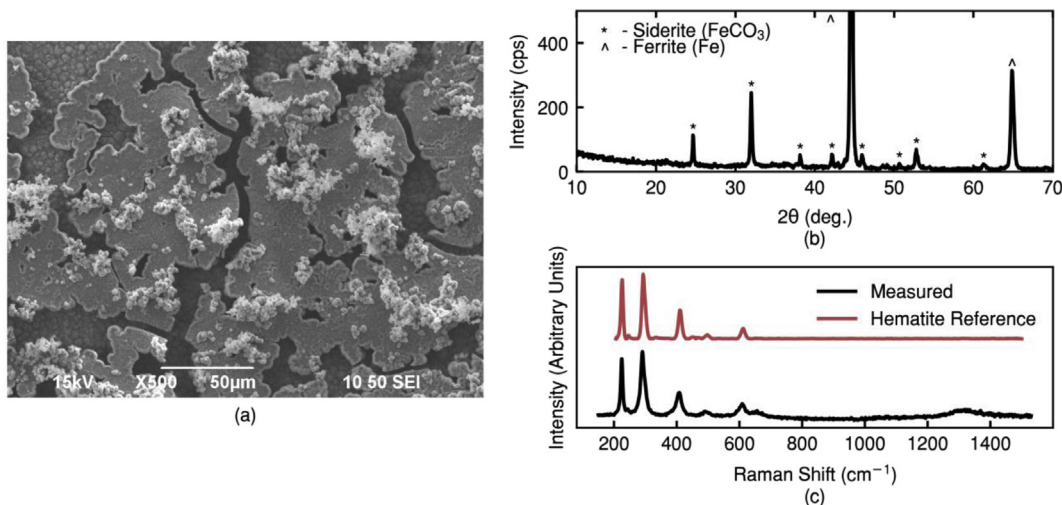


**Fig. 11.** Effect of  $O_2$  on (a) SEM corrosion product morphology and compositional analysis with (b) XRD and (c) Raman spectroscopy. XRD peak labels correspond to siderite (\*) and ferrite (△). The hematite Raman spectrum is included as a reference.

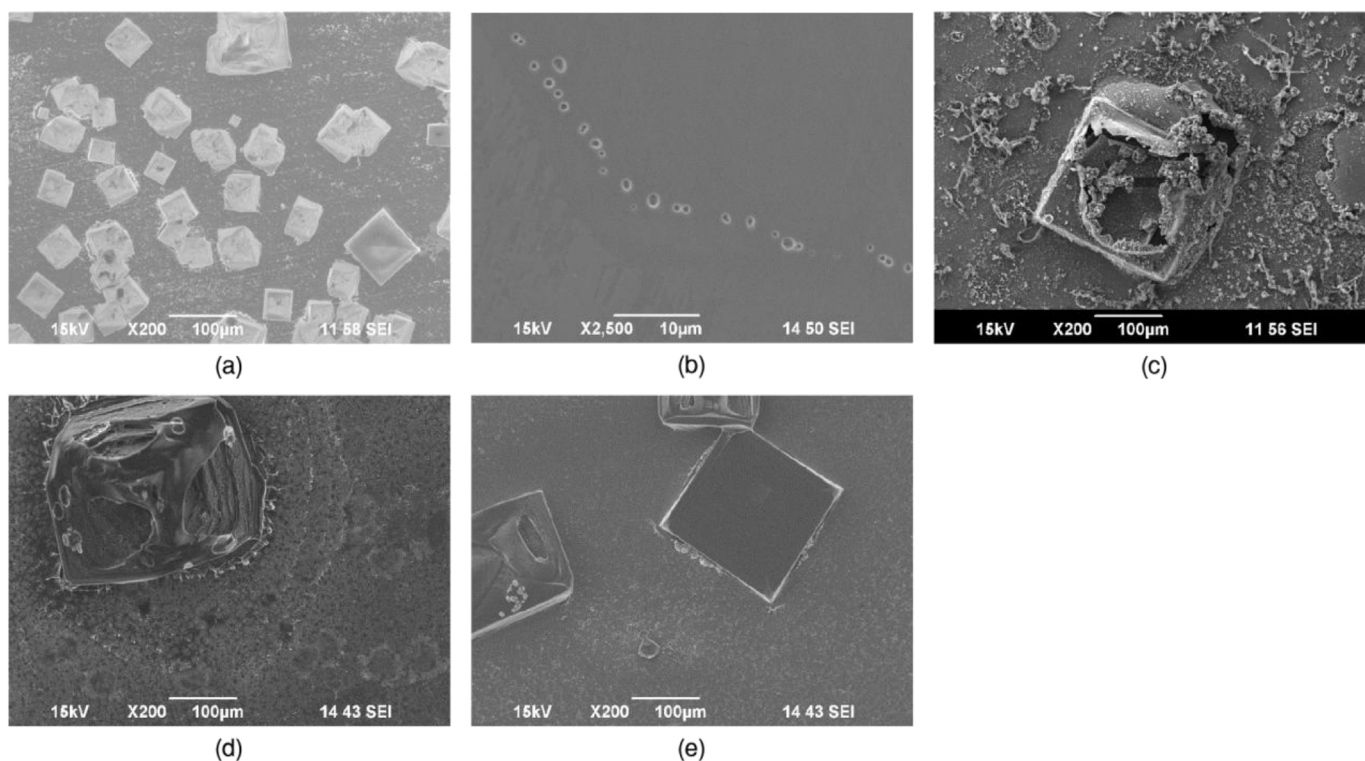


Fig. 12. SEM surface microscopy of (a) layer prior to exposure, (b) slight corrosion caused by the salt-drying process, and after a 3-day exposure to a 0.3 mbar H<sub>2</sub>S, 0.97 bar CO<sub>2</sub> atmosphere at (c) 75%, (d) 58%, and (e) 33% relative humidity.

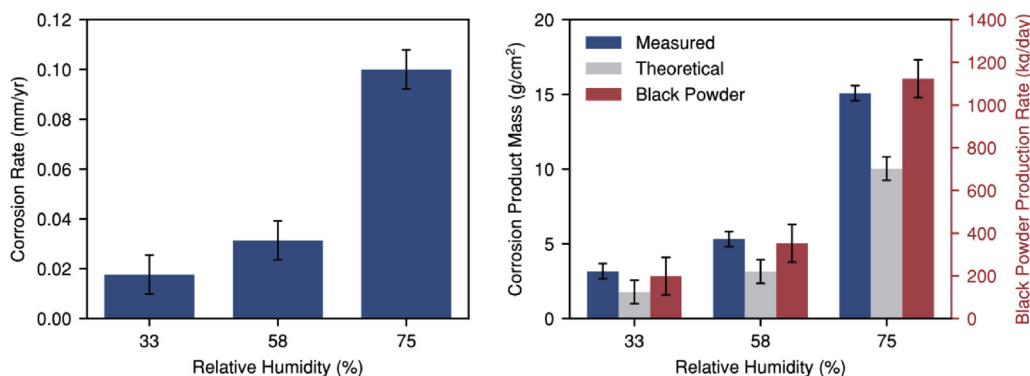


Fig. 13. Effect of RH on corrosion rate, corrosion product mass (left axis), and maximum allowable black powder production rate (right axis). The calculation for black powder production rate assumes a 42 in. (1.07 m) ID, 100 km pipeline.

**Acknowledgements**

The authors would like to thank the Gas Research Center (Project GRC11007), The Petroleum Institute, Abu Dhabi, UAE for their

financial support, Mr. Cody Shafer for apparatus drawings, Prof. Srdjan Nescic for insightful discussions, and the Center for Electrochemical Engineering Research at Ohio University for access to the XRD and Raman systems.

**Appendix A**

The difference between the measured and theoretical corrosion product masses offers a means of determining how much corrosion product was removed from the surface of the steel specimens as solid corrosion product (i.e., black powder) or ionic species in the condensate which drips away. The methodology for the calculation of the measured and theoretical corrosion products, and the expected black powder production rates, are described herein.

Specimen mass measurements (g) were taken before exposure ( $m_i$ ), immediately after exposure ( $m_e$ ), and after the corrosion product was removed ( $m_f$ ). The measured mass of corrosion product,  $\tilde{m}_{meas}$  (g/m<sup>2</sup>), is then the difference in specimen mass before and after the corrosion product was removed, and then normalized by specimen area (m<sup>2</sup>):

$$\tilde{m}_{meas} = \frac{m_e - m_f}{A_s} \tag{A-1}$$

The theoretical corrosion product mass considers what the corrosion product mass would have been if all the material removed by the corrosion

process stayed on the specimen surface as a solid corrosion product. This corrosion product would then consist of iron carbide, the other alloying species such as Mn, Ni, Mo, etc., and the carbonates, sulfides, and/or oxides formed dependent upon the corrosion environment.

The mass of iron carbide is calculated by:

$$m_{\text{Fe}_3\text{C}} = \frac{-\Delta m x_{\text{C}} M_{\text{Fe}_3\text{C}}}{M_{\text{C}}} \quad (\text{A-2})$$

where  $\Delta m = m_f - m_i$ ,  $x_{\text{C}}$  is the mass fraction of carbon in the steel, and  $M_i$  is the molar mass of species  $i$ . This equation assumes that all carbon in the steel is in the form of iron carbide. Realistically, there is carbon dissolved in the steel, however this portion is assumed to be negligible. The mass of the other species denoted in Table 2 is:

$$m_{\text{other}} = - \sum_{i=\text{Mn, Ni, Mo, ...}} \Delta m x_i. \quad (\text{A-3})$$

The mass of the iron-containing phases in the corrosion product will depend upon the environment. For these calculations,  $\text{FeCO}_3$  was assumed in the absence of  $\text{H}_2\text{S}$  and  $\text{O}_2$ ,  $\text{FeS}$  was assumed if  $\text{H}_2\text{S}$  was present, and  $\text{Fe}_2\text{O}_3$  was assumed under oxic conditions. This mass must also account for the iron in iron carbide, so the final mass of corrosion product consisting of species  $j$  is given by:

$$m_j = \frac{-\Delta m M_j \left( \frac{x_{\text{Fe}}}{M_{\text{Fe}}} - \frac{3x_{\text{C}}}{M_{\text{C}}} \right)}{n} \quad (\text{A-4})$$

where  $n$  is moles of iron per mole of corrosion product  $j$ . Finally, the theoretical corrosion product mass,  $\tilde{m}_{\text{theor}}$ , is calculated by:

$$\tilde{m}_{\text{theor}} = \frac{m_j + m_{\text{Fe}_3\text{C}} + m_{\text{other}}}{A_s}. \quad (\text{A-5})$$

The black powder production rate,  $\dot{m}_{\text{BP}}$  (kg/day), is extrapolated from the theoretical corrosion product mass over the internal surface area of a straight, 100 km, 42 in. (1.07 m) pipe ( $A_{\text{pipe}}$ ,  $\text{m}^2$ ) and converted to a rate by dividing by the experiment duration,  $t$  (days):

$$\dot{m}_{\text{BP}} = \frac{\tilde{m}_{\text{theor}} A_{\text{pipe}}}{t} 10^{-3} \quad (\text{A-6})$$

## References

- Baldwin, R., 1997. Black Powder in the Gas Industry - Sources, Characteristics and Treatment (No. TA 97-4). Mechanical and Fluids Engineering Division Southwest Research Institute, San Antonio.
- Bedworth, R.E., Pilling, N.B., 1923. The oxidation of metals at high temperatures. *J. Inst. Met.* 29 (3), 529–582.
- Bhardwaj, A., Kumar, B., Prasad, S., Srivastava, S.K., 2016. Characterization of black powder in gas pipelines. *Mater. Perform.* 55 (8), 54–59.
- Bird, R.B., Stewart, W.E., Lightfoot, E.N., 2007. *Transport Phenomena*, 2. ed. Wiley, New York.
- Birks, N., Meier, G.H., Pettit, F.S., 2006. *Introduction to the High Temperature Oxidation of Metals*, Second Edition, second ed. Cambridge University Press.
- Golightly, F.A., Stott, F.H., Wood, G.C., 1979. The relationship between oxide grain morphology and growth mechanisms for Fe-Cr-Al and Fe-Cr-Al-Y alloys. *J. Electrochem. Soc.* 126 (6), 1035–1042. <https://doi.org/10.1149/1.2129170>.
- Hali, A.L., Lehmann, M.N., Cook, S.E., Russell, R.D., Hartley, S.J., Finan, S.M., 2016. The use of preservation chemicals for extended shut-ins following hydrostatic testing of gas and service pipelines. In: *Offshore Technology Conference Asia*, . <https://doi.org/10.4043/26581-MS>.
- Holden, J., Hansen, A., Furman, A., Kharshan, R., Austin, E., Corporation, C., Lake, W.B., 2010. Vapor corrosion inhibitors in hydro-testing and long term storage applications. In: *Corrosion*. NACE International, Houston, pp. 1–14.
- Khan, T.S., Al-Shehhi, M.S., 2015. Review of black powder in gas pipelines – an industrial perspective. *J. Nat. Gas Sci. Eng.* 25, 66–76. <https://doi.org/10.1016/j.jngse.2015.04.025>.
- Khan, T.S., Alshehhi, M., Stephen, S., Khezzer, L., 2015. Characterization and preliminary root cause identification of black powder content in a gas transmission network – a case study. *J. Natural Gas Sci. Eng.* 27 (Part 2), 769–775. <https://doi.org/10.1016/j.jngse.2015.09.022>.
- Kofstad, P., Lillerud, K.P., 1980. On high temperature oxidation of chromium II. Properties of and the oxidation mechanism of chromium. *J. Electrochem. Soc.* 127 (11), 2410–2419. <https://doi.org/10.1149/1.2129481>.
- Kolts, J., 2004. *Design for Internal Corrosion Resistance of Sales Gas Pipelines*. Nice, France.
- Lennie, A.R., Redfern, S.A.T., Schofield, P.F., Vaughan, D.J., 1995. Synthesis and Rietveld crystal structure refinement of mackinawite, tetragonal FeS. *Mineral. Mag.* 59 (397), 677–684.
- Lillerud, K.P., Kofstad, P., 1980. On high temperature oxidation of chromium I. Oxidation of annealed, thermally etched chromium at 800°–1100°C. *J. Electrochem. Soc.* 127 (11), 2397–2410. <https://doi.org/10.1149/1.2129478>.
- Litke, W., Bojes, J., Blais, P., Lerbscher, J., Wamburi, W., 2013. *Aggressive Corrosion Associated with Salt Deposits in Low Water Content Sour Gas Pipelines* (Vol. Paper No.). NACE International, Houston, TX.
- NACE MR0175, 2015. NACE International.
- Olabisi, O., Al-Sulaiman, S., Jarrah, A., Khuraibut, Y., Mathew, A., 2017. Black powder in export gas lines. *Mater. Perform.* 56 (4), 50–54.
- Schindelholz, E., Risteen, B.E., Kelly, R.G., 2014. Effect of relative humidity on corrosion of steel under sea salt aerosol proxies I. *NaCl. J. Electrochem. Soc.* 161 (10), C450–C459.
- Sherik, A.M., Zaidi, S.R., Tuzan, E.V., Perez, J.P., 2008. Black powder in gas transmission systems. In: *CORROSION*, vol. 2008 NACE International.
- Sridhar, N., Dunn, D.S., Anderko, A.M., Lencka, M.M., Schutt, H.U., 2001. Effects of water and gas compositions on the internal corrosion of gas pipelines—modeling and experimental studies. *Corrosion* 57 (3), 221–235. <https://doi.org/10.5006/1.3290347>.
- Standard Practice for Preparing, Cleaning and Evaluating Corrosion Test Specimens, 2011. (No. ASTM Standard G1–03).
- Sun, W., Nešić, S., 2009. A mechanistic model of uniform hydrogen sulfide/carbon dioxide corrosion of mild steel. *Corrosion* 65 (5), 291–307.
- Yaakob, N., Farelis, F., Singer, M., Nesic, S., Young, D., 2016. Localized Top of the Line Corrosion in Marginally Sour Environments. pp. 1–14 (Vol. Paper No.
- Yamada, J., Kaneta, H., Nakayama, K., 2011. Analysis of black powder in natural gas pipelines. In: *Proceedings* (p. Paper 11088). Houston, TX.
- Zhao, K., Gu, T., Cruz, I., Kopluku, A., 2010. Laboratory investigation of MIC in hydro-testing using seawater. In: *Corrosion*. NACE International, Houston.